ELSEVIER

Polymer 41 (2000) 5283–5296

polymer

Characterization of a polyamide-6-based intumescent additive for thermoplastic formulations

M. Le Bras*, S. Bourbigot, E. Félix, F. Pouille, C. Siat, M. Traisnel

Laboratoire de Génie des Procédés d'Interaction Fluides Réactifs-Matériaux, E.N.S.C.L., USTL, BP 108, F-59652 Villeneuve d'Ascq Cédex, France

Received 9 February 1999; accepted 5 October 1999

Abstract

Charring polymers may be used as carbonization agents in fire retardant (FR) intumescent additive master batches. This paper presents typical polyamide-6-based master batches which are extensively used in polyethylenic FR formulations. It is shown that a blend of polyamide-6 and an ethylene–vinyl acetate copolymer allows the incorporation of the carbonization catalyst, i.e. ammonium polyphosphate, in the polymeric material. The problem of the migration of the phosphate throughout the polymeric matrix is discussed. Solid state NMR spectroscopy is presented as a tool to predict and to explain the part played by the interfacial agent, i.e. the functionalized polymer. © 2000 Elsevier Science Ltd. All rights reserved.

Keywords: Ammonium polyphosphate; Polyamide-6; Ethylene vinyl acetate copolymer

1. Introduction

The large diffusion of polymeric materials, which occurred in the last few decades, has increased fire risks. In particular, use of polyolefins in electrical, building or transport applications are often limited because of their bad fire properties.

The most effective fire retardant (FR) systems are halogen-based materials [1–4]. These systems are known to be a source of corrosive, obscuring and toxic smoke when the products burn [5–8]. As a result, the present trend aims at the limitation of the use of halogen-based FR systems. Research and development turn towards halogen-free FR formulations [9,10].

A solution to limit the kinetics of the combustion mechanism of polymers consists in developing on the outer surface of the polymer a glassy [11] or an expanded shield [12] which may, at least partially, limit the transfer of fuel to the gas phase, the transfer of heat from the gaseous phase to the condensed phase and eventually oxygen diffusion in the condensed phase.

Several FR intumescent polyolefin-based formulations have been developed in our laboratory. Their protection is carried out by the formation in the conditions of a fire of an intumescent coating, i.e. the formation of an expanded carbonaceous structure on the flame front [13,14]. Intumescent additive formulations are generally mixtures of carbonization agents and carbonization catalysts (products such as phosphoric acids and/or boric acid salts which form stable acidic species on heating) and eventually, a blowing agent. Previous studies have shown that the intumescent structure mainly consists in polyaromatic species which structure grows when the temperature increases [15].

It also has been shown that the polyamide-6 (PA-6)/ammonium polyphosphate (APP) additives mixture leads to FR properties of interest, by developing an intumescent shield [16,17]. The effect of the fire retardant ammonium polyphosphate on the thermal degradation of aliphatic polyamides has already been studied [17]. A chemical interaction is shown which takes place between APP and PA-6 on heating, resulting in destabilization of PA-6 and modification of its degradation behavior. The intumescent phenomenon induced by APP is held for responsible for the fire retardant behavior of the blend in which the polyamide plays both the role of the polymeric matrix and of a carbonization agent.

Most recently, we have developed mixtures of APP and PA-6 for use as additives in thermoplastic formulations. These formulations are especially interesting taking into account their low additive loading and consequently the preservation of the mechanic properties of interest of the matrices.

Unfortunately, the stability (the compatibility of APP

* Corresponding author. Tel.: +33-3-20436906.
E-mail address: michel.le-bras@ensc-lille.fr (M. Le Bras).

PII: S0032-3861(99)00736-3

Nomenclature

a	Average of the distance between two protons (nm)
APP	Ammonium polyphosphate
$\bar{b}_{3D}$	Size of the slow relaxation domains (nm)
C	Torque (N m/rad)
D	Spin-diffusion coefficient (cm^2/s)
e	Weibull coefficient
EVA8	Ethylene vinyl acetate copolymer (8 wt% of vinyl acetate)
EVA24	Ethylene vinyl acetate copolymer (24 wt% of vinyl acetate)
FR	Fire retardant
H	Length (m)
K_1, K_2, Y	Constants
LOI	Limiting oxygen index (vol%)
M	Magnetization amplitude (%)
M_{OC}, M_{OL}	Fast and slow magnetization amplitudes (%)
n	Pseudo-plasticity index
PA-6	Polyamide-6
S	Area (m^2)
t	Time (s)
T_1	Spin–lattice relaxation time (μs)
T_2	Spin–spin relaxation time (μs)
T_{2C}, T_{2L}	Fast and slow spin–spin relaxation time (μs)
V	Rotation rate of the rheometer blade (rpm)

Greeks

γ	Speed gradient (s^{-1})
η	Apparent value of the viscosity (Pa s)
τ	Strain (Pa)

with PA-6) of the PA-6/APP blends obtained directly mixing the APP in melted PA-6, is low: a migration of the mineral salt occurs during solidification of the melt and versus time in the solid. As an illustration of this migration, Fig. 1 presents the MEB picture of the surface of a PA-6/APP blend sheet which reveals the presence of the APP grains out of the sheet after 15 days at 25°C in dry air.

Such a migration may be avoided using a compatibilizer (ethylene–vinyl acetate copolymer [18,19], functionalized terpolymers of ethylene, siloxane or silane-based resins [20]). Among these compatibilizers, ethylene–vinyl acetate copolymer (EVA8) has been selected. The LOI values [21] and the UL-94 classification [22] for different ratios of APP in the blend PA-6/EVA8 (weight ratio 6:1) are shown in Table 1 and Fig. 2. They show that FR performances of interest are obtained using at least 28 wt% of APP and that EVA8 plays the part of a synergistic agent.

The PA-6/EVA8/APP system has been tested as an FR additive in several thermoplastics matrices such as polypropylene [23], polystyrene [18] and ethylene–vinyl acetate copolymers [19]. It has been shown that interesting FR

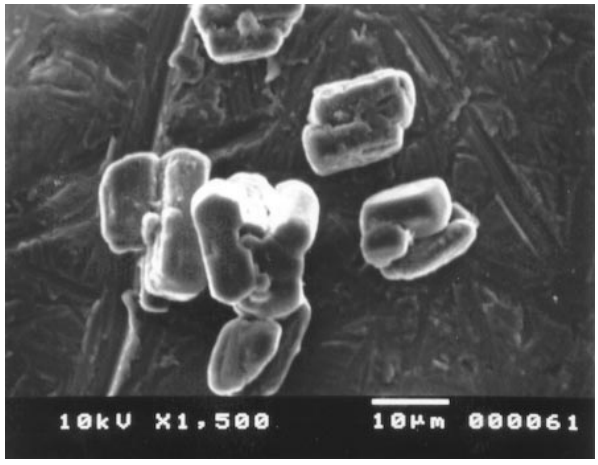

Fig. 1. MEB image (secondary electron picture) of the PA-6/APP surface.

performances (LOI ≥ 30 vol%, V0 rating and heat release rate (RHR; measured by oxygen consumption calorimetry according to NBS-IR 82:2604 [24]) lower than 400 kW/m^2) are obtained using a 40 wt% addition of PA-6/EVA8/APP in the polymers. Fig. 3 illustrates the FR performances resulting of the addition of the PA-6/EVA/APP system in an ethylene–vinyl acetate copolymer (EVA24; 24 wt% of vinyl acetate). The corresponding materials (EVA24/PA-6/APP) presents LOI = 32 vol% and V0 rating. Fig. 4 shows that substitution of conventional additives systems, such as $Al(OH)_3$ coated by a silane sizing agent, allows at least partially the preservation of the mechanical properties of the host polymeric matrix.

For all polymer/PA-6/EVA8/APP systems, the FR performance is reached via the formation of an intumescent coating (charring and bubbling), PA-6 charring occurs at the temperature of the beginning of its thermo-oxidative degradation [26,27]. So, the PA-6/EVA8/APP (PA-6/EVA8 = 6/1 w/w, 28 wt% of APP; noted PA-6/EVA8/APP in the paper) appears to be a powerful intumescent FR additive. Moreover, the addition of ethylene–vinyl acetate is responsible for both a synergistic effect and a limitation of the exudation phenomenon [28,29]. The aim of this work is then to study the processing of the blend using a ethylene–vinyl acetate copolymer in order to maximize the interfacial bonding and to prevent the reject of the mineral additive throughout the polymer matrix.

In a first part, the conditions of the master batch process will be discussed. The chemical and structural evolution of

Table 1
LOI values and UL-94 rating of PA-6 based formulations versus their composition

Formulation	LOI (vol%)	UL-94
PA-6	21	No rating
PA-6/EVA8 (6/1 w/w)	20	No rating
PA-6/APP (28 wt%)	24	No rating
PA-6/EVA8/APP (28 wt%)	29	V0 rating

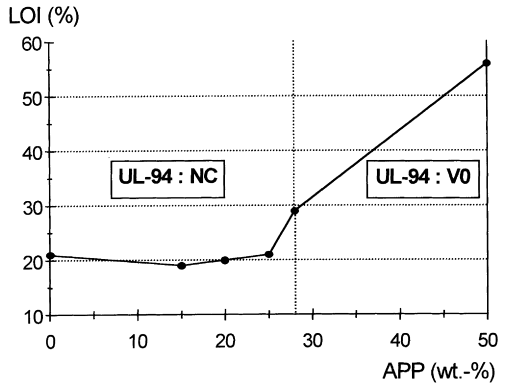

Fig. 2. LOI values and the UL-94 rating of the PA-6/EVA8/APP formulations versus their APP content.

the polymer phases in the PA-6/APP and PA-6/EVA8/APP will be then compared using X-ray diffraction spectroscopy (XRD), X-ray photoelectron spectroscopy (XPS) and electron spin resonance (esr). Finally, the materials will be examined using solid state NMR spectroscopy to predict and to explain the part played by the compatibilizer (i.e. EVA8 acting as a sizing agent of APP). Additional structural information will be obtained from low resolution ^{1}H NMR of the solid state. The shape of the free induction decay (FID) allows the measurement of the spin–spin relaxation times (T_2) after solid echo sequences. The size measurement of the slow relaxation domains will then be examined using as "probe" the free precession of the protons and the spin diffusion phenomenon in the materials.

2. Experimental

2.1. Materials

Raw materials were polyamide-6 (PA-6, as pellets supplied by Rhône-Poulenc), ethylene–vinyl acetate copolymer (EVA8, Lactene 1005 VN3, melt index: 0.4 g/10 mn, as pellets supplied by Elf Atochem) and ammonium polyphosphate (APP, Exolit 422, soluble fraction in $H_2O < 1$ wt%, powder supplied by Clariant). The study has been carried out using the PA-6/EVA8 blend for the ratio PA-6/EVA8 = 6 (w/w) with addition of 28 wt% of APP.

Materials were melt mixed at 230, 235 and 240°C using the Brabender Mixer measuring head (type 350/EH, roller blades, checking of the mixing conditions using the data processing torque rheometer system Brabender Plasticorder PL2000, constant shear rate: 50 rpm) which allows to establish the steady state conditions (temperature, torque) of the mixing process. Sheets ($100 \times (00 \times 3$ mm^3) were then obtained using a Darragon pressing machine at 220°C and at a pressure of 10^6 Pa.

2.2. Rheological properties

Assimilating the Brabender Laboratory mixer to a rotary rheometer with co-axial cylinders, approximate melt rheological properties of the polymeric mixture can be calculated directly from torque rheometer data [30–32]: the constraint τ sustained by the material is connected to the motor torque C by the relation:

$$C = \tau \times S \times R$$

Determination of the apparatus constants allows us to propose the apparent viscosity–torque linear relation:

$$\eta = \frac{\tau}{\dot{\gamma}} = 1417.8 \times \frac{C}{V}$$

(C in N m/rad, $V = 50$ rpm in our conditions)

which allows us to consider that variations of the experimental

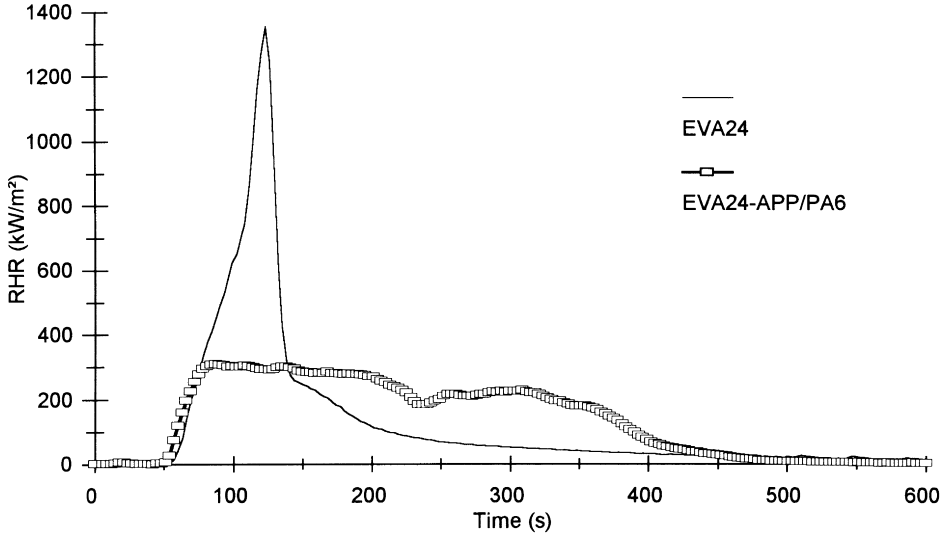

Fig. 3. Comparison of the heat release rate for EVA24 and EVA24/PA-6/APP (external heat flux: 50 kW/m^2), from Bourbigot et al. [25].

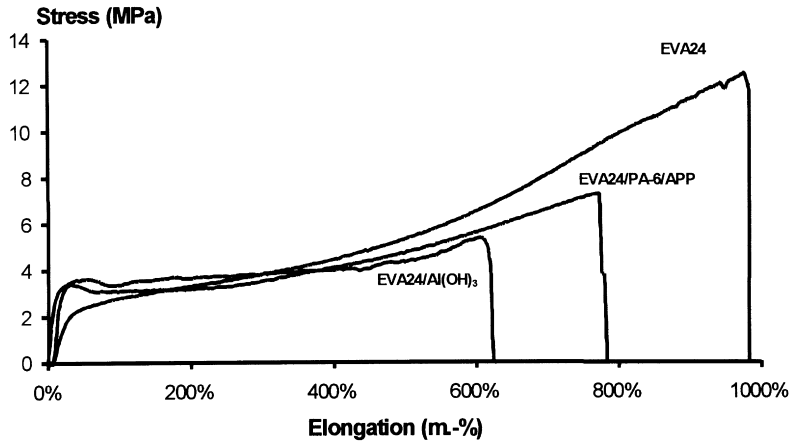

Fig. 4. Comparison of the elongation at break of EVA24, EVA24/PA-6/APP and EVA24/$Al(OH)_3$, from Bourbigot et al. [25].

torque are representative of variations of the apparent viscosity [33,34].

2.3. Chemical analyses

The amounts of carbon and hydrogen were determined by burning the samples in an excess of oxygen at 1050°C. The quantity of the evolved CO_2 was then determined by coulometry and was proportional to the total quantity of carbon in the sample. The quantity of evolved water condensed as liquid or ice at 0 ± 2°C was determined making a stoichiometric reaction between coal and water to form CO which was transformed to CO_2 on copper oxide at 1120°C. The amount of evolved CO_2 was then determined as above. The phosphorus content was evaluated by mineralization in aqueous medium and then dosed by plasma emission spectrometry.

The surface of the polymeric samples were examined using XPS on a AEI ES 200B spectrometer using AlK_α ($h\nu = 1486.6$ eV). The spectrometer was run in a fixed analyzer transmission mode at a pass energy of 65 eV with an X-ray power source of 250 W. Under these conditions, the full-width at half-maximum (FWHM) of the Au 4f peak is 1.4 eV. Samples were mounted by pressing into the indium holder and introduced in a pre-chamber to obtain a pressure of 1.3×10^2 Pa. In the main analyzer chamber, the pressure was between 10^{-5} and 10^{-6} Pa. It was necessary to cool the samples to around -70°C to avoid any degradation of the material. Data acquisition considering C_{1s}, P_{2p} and N_{1s} spectra, was controlled by a AEI DS 200B data system connected to a computer. To compensate for sample charging all binding energies were referenced to C_{1s} at 285 eV. The peaks were resolved using peak analysis software (Peakfit of Jandel Scientific) assuming a Lorentzian/Gaussian line shape [35].

2.4. Scanning electron microscopy (SEM)

The specimens observed were fractured in liquid nitrogen. After coating the fracture surfaces with carbon, their observations were carried out with a Jeol 5300 scanning electron microscope (acceleration voltage: 10 kV). EVA containing domains may be observed after a selective dissolution of the PA-6 phase using methanoic acid (48 h at 25°C).

2.5. X-ray diffraction (XRD)

The XRD spectra were recorded with an automatic Siemens D5000 X-ray spectrometer using the Cu $K\alpha_{1,2}$ radiation and a nickel filter ($\lambda = 0.15406$ nm) in the range $5° < 2\theta < 55°$. These tests were carried out on sheets (3 mm thickness) with a rotation of the sheets to suppress structural orientation effects. Diffract AT software allows then subtracting the $K\alpha_2$ radiation component, smoothing of the spectra, subtracting the amorphous zone scattering signal, measuring the peaks intensity, and, finally, evaluating the X-ray penetration. The Bragg and the Debye–Scherrer laws [36] are used to determine the particles size.

2.6. Electron spin resonance (esr)

All esr spectra were recorded at 25°C using the dual-sample cavity "E 190" of the spectrometer Varian "E Line" (klystron frequency about 9.5 GHz (X band), modulation frequency: 10^5 Hz) with a sweep width of 0.04 T about a central frequency of 0.34 T. Constant experimental acquisition parameters in common were a modulation amplitude of 4×10^{-6} T, a conversion time of 10 ms and a RC filter time constant of 64 ms. The incident adequate microwave power was selected weak to avoid signal saturation and linewidth broadening. Splitting spectroscopic factor (g) and free radicals concentrations were calculated referring to a standard ("strong pitch" supplied by Bruker, $g = 2.0023$ and spin concentration: 3×10^{15} spins/cm). Spectroscopic functions fitting with the signal are generally either Lorentzian, Gaussian or Voigt (combination of Lorentzian and Gaussian functions) functions. The concentrations of the paramagnetic species were in that case,

computed using a method of double integration of the area of the spectra [37].

2.7. Solid state NMR

High resolution NMR spectra of the solids were performed on a Bruker SX 100 weak field spectrometer at a spinning speed of 3 kHz and using a Bruker probe head equipped with a 7 mm MAS assembly. ^{31}P NMR measurements were performed at 40.5 MHz with magic-angle spinning (MAS), with high power ^{1}H dipolar decoupling (DD) and a repetition time of 450 s (because of the long spin–lattice relaxation time: $T_1 \approx 80$ s). All spectra were acquired as a result of 512 scans. The reference used was 85% H_3PO_4 in aqueous solution. ^{13}C NMR measurements were performed at 25.2 MHz (2.35 T) with MAS, high power ^{1}H decoupling and ^{1}H–^{13}C cross polarization (CP). The Hartmann–Hahn matching condition was obtained by adjusting the power on ^{1}H channel for a maximum ^{13}C FID signal of adamantane. All spectra were acquired with contact times of 1 ms. A repetition time of 10 s was used. Typically, 2048 scans were necessary to obtain spectra with a good signal/noise ratio and the reference used was tetramethylsilane.

Low resolution ^{1}H NMR studies were carried out using a Bruker SX 100 spectrometer, operating at a proton frequency of 100.13 MHz and with a 7 mm solenoid probe. The method of inversion recovery $[\pi$–τ–$\pi/2]$ was used to measure proton spin–lattice relaxation times (T_1). The computation of T_2 was made using a solid echo sequence $[(\pi/2)_x$–τ–$(\pi/2)_{-x}]$ [38]. After the first 90° pulse, a second 90° pulse is applied to the system after an interval that is slightly longer than the dead time of the spectrometer (15 μs). This generates an echo which would retain the shape of the free-induction decay (FID). We may consider that the FID lineshape after a solid echo pulses is a reasonable approximation of the true FID.

In a heterogeneous material, it is possible to observe the effects of the spin diffusion with a Goldman–Shen pulse sequence $[(\pi/2)_x$–t_0–$(\pi/2)_x$–τ–$(\pi/2)_x]$ [39]. The magnetization of each material shows a two-component FID with significantly different T_2. The fixed time t_0 is chosen such that M_2, which has a shorter T_2, has decayed to zero while there is still sufficient magnetization M_1 remaining in the domain of slow relaxation. Assuming that $t \ll T_1$, the recovery factor $R(t)$ may be formally written as Eq. (1) [40]:

$$R(t) = \frac{M_2(t)}{M_2(t \to \infty)} \tag{1}$$

The theoretical considerations of $R(t)$ have been previously presented by Cheung et al. [40] and the principal conclusions of their work relevant to these studies are summarized here. In solids, the magnetization transfer via spin diffusion is described by:

$$\frac{\partial m(r,t)}{\partial t} = D\nabla^2 m(r,t) \tag{2}$$

with m the local magnetization density at the point r and at a time t.

Assuming that $t \ll T_1$ and that the spin diffusion coefficient D is a constant in the whole of the sample [41], solving Eq. (2) leads to:

If b distribution follows a Poisson law:

$$P(b) = \frac{1}{\bar{b}} \times \exp\left(-\frac{b}{\bar{b}}\right) \tag{3}$$

with b the mean size of domain of slow relaxation.

The $R(t)$ curve in a three-dimensional model may be expressed as

$$R(t) = 1 - \left[\exp\left(\frac{Dt}{\bar{b}^2}\right)\operatorname{erfc}\left(\frac{Dt}{\bar{b}^2}\right)^{1/2}\right]^{\alpha} \tag{4}$$

with $\alpha = 1$, 2 and 3 and erfc a complementary error function.

If b distribution follows a Gaussian law:

$$P(b) = \frac{2}{\pi\bar{b}}\exp\ -\frac{1}{\pi}\left(\frac{b}{\bar{b}}\right)^2 \tag{5}$$

with

$$R(t) = 1 - \left\{\frac{2}{\pi^{1/2}}\left[\left(\frac{Dt}{\bar{b}^2} + \frac{\pi}{4}\right)^{1/2} - \left(\frac{Dt}{\bar{b}^2}\right)^{1/2}\right]\right\}^{\alpha} \tag{6}$$

However, the computation of $R(t)$ is possible if the spin diffusion coefficient D is known. In this study

$$D = 0,13a^2/T_{2C} \tag{7}$$

is used with T_{2C} the spin–spin relaxation time of the rigid phase and a the lattice constant.

In the particular case of the intumescent PA-6-based formulations, a is one of the lattice parameters of PA-6 computed from the XRD spectra. Indeed, the crystalline phase of PA-6 shows a monoclinic structure ($a \neq b \neq c$, $\alpha = \gamma, \beta = 112.5°$). The measurement of inter-reticular distance d_{200} allows to propose: $a = d_{200}/\sin(67.5°)$.

3. Results and discussion

3.1. Processing conditions

Apparent values of the viscosity (Fig. 5) show that APP plays different roles versus temperature and content in the melts. With a content lower than 25 wt%, it acts as a plasticizer at 230 and 235°C and as an hardener at 240°C. Moreover, it always acts as an hardener at 230 and 235°C when its contents are higher than 28 wt%.

The apparent viscosity is nearly a constant at 240°C. This behavior in the processing conditions may be explained either by a reaction between the PA-6 and APP (previously studied by Levchik et al. [42,43] or by the first step of the degradation of the EVA8 (evolution of acetic acid via the degradation of the vinyl acetate groups [44]). Moreover, mechanical and thermal strains applied on the material

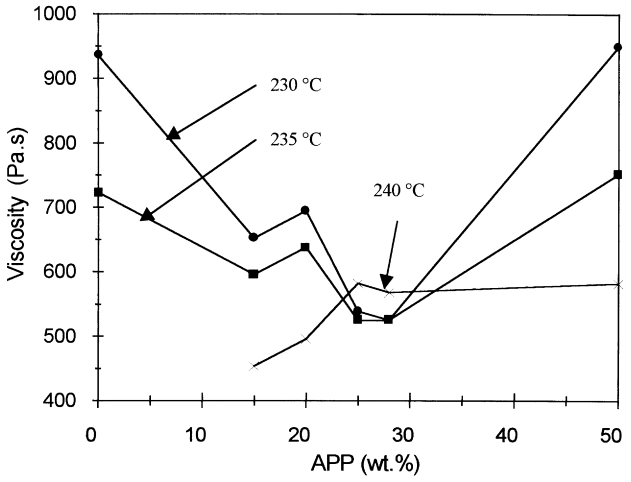

Fig. 5. Rheological data of the melt mixing process of PA-6/EVA8/APP versus temperature and APP content.

during mixing leads to the breaking of the polymers chains with free radicals formation and subsequent formation of links between the linear chain of the polymers. Fig. 6 presents the esr spectrum of PA-6/EVA8/APP after a mixing process at 240°C. It shows a complex signal which may be assigned to the presence of several radical species in the material. Fit of the integrated signal verifies this hypothesis, the signal corresponds in fact to the superposition of several nearly Lorentzian signals difficult to assign (Fig. 7). The fit shows a signal at $H = 0.338$ T which increases slowly with time of the mixing process and sharply when the temperature increases. A g_{eff} value is deduced which is close to 2.03 and may be assigned to free radicals trapped in an aromatic and/or polyaromatic structure [45,46] previously observed in intumescent FR polypropylene-based formulations [14]. It implies the beginning of the carbonization process during mixing at 240°C.

The polymer blend does not present the behavior of a thermoplastic resin when $25 < \text{APP} < 28$ wt%, its apparent viscosity remain the same at the three mixing temperatures. It suggests an important chemical modification of the blend which may be explain by the same chemical reaction between APP and PA-6. This behavior is important because LOI of intumescent material depends on the stability of the

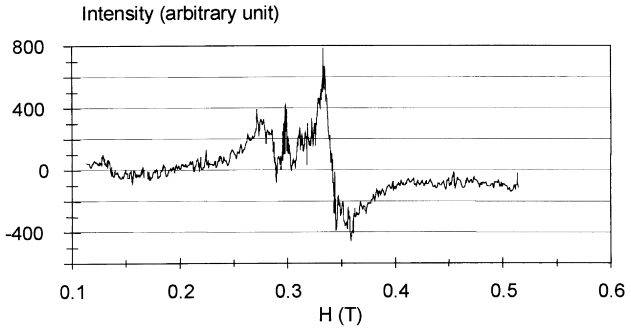

Fig. 6. esr spectrum of PA-6/EVA8/APP processed at 240°C.

protective coating upon the virgin material; This latter is severely affected by melting and dripping; more, the UL-94 test considers dripping as a criterion for rating. So, the optimized FR properties of PA-6/EVA8/APP (APP relative concentration: 28 wt%) may be explained by the particulate dynamic property of this blend.

The study will then be carried out with specimens mixed at 235°C, this temperature corresponding to the best compromise: as a matter of fact, the homogeneity of the samples is assured at this temperature which does not allow a dramatic development of the carbonization reaction.

3.2. Chemical characterization

Chemical analyses allows to compare initial P/C atomic ratio of the initial raw materials mixture and of the blends after processing and aging of the blend sheets in the laboratory conditions during three months (Fig. 8).

The two ratios are very close to each other, especially for an APP concentration lower than 28 wt%. This result confirms that addition of EVA8 in the blend leads to a compatibilizing effect. Beyond this percentage, a light throwing up of APP from the blend during processing and bleaching during aging are observed.

The comparative SEM study of PA-6/APP and PA-6/EVA8/APP (test sheets fractured at liquid nitrogen temperature, Fig. 9) confirms the compatibilizing effect of EVA8 addition. Indeed, picture of the fracture of PA-6/APP shows the APP agglomerate in the fracture zone when such agglomerate is not observed with PA-6/EVA8/APP. It may be proposed that EVA8 avoids the migration of APP in the PA-6 matrix when a strain is applied because the APP particles are perfectly embedded in the polymeric matrix.

The picture of the PA-6/EVA8/APP fracture zone after selective dissolution of the PA-6 phase shows that the APP particles remain embedded in a polymeric phase and that the nearly spherical nodules observed in Fig. 8b are preserved. This result specifies the localization of EVA both in the periphery of the APP grains and in nodules characteristic of mixture of two polymers with very different viscosity and which are not miscible [47].

The X-ray photoelectron spectroscopy characterization of the surface of the materials (APP grains, PA-6 and PA-6/EVA8/APP molded sheets) shows that the N_{18} binding energy of PA-6/EVA8/APP is closer to the APP one than to the corresponding value with PA-6 (Table 2) and that the

Table 2
Nitrogen and phosphorous binding energies in APP, PA-6 and PA-6/EVA8/APP

Samples	Nitrogen binding energy (eV)	Phosphorous binding energy (eV)
APP	402.1	135.0
PA-6	399.7	–
PA-6/EVA8/APP	401.9	134.9

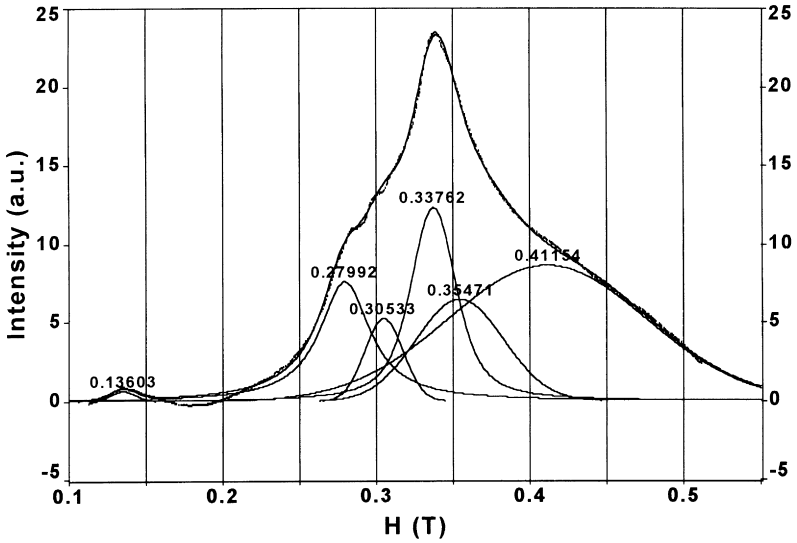

Fig. 7. Fit of the esr spectrum of PA-6/EVA8/APP processed at 240°C (selected distribution of the signal: Voigt function).

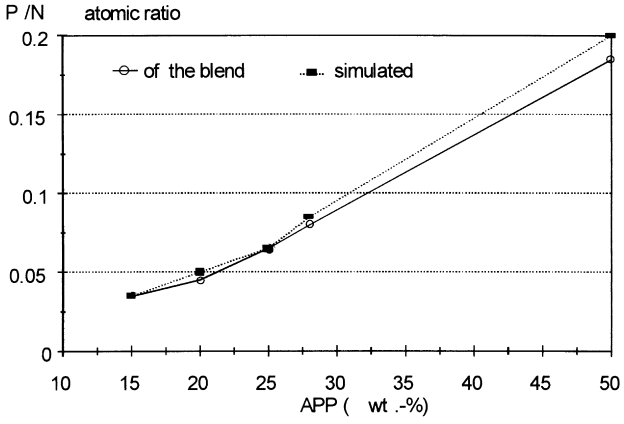

Fig. 8. Comparison between atomic P/C ratio in the raw material mixture (simulated) and the P/C ratio of the blends (deduced from chemical analysis, after aging three months under laboratory conditions).

P_{2p} binding energy with PA-6/EVA8/APP is close to this with APP. This last result implies that surface APP does not react strongly with PA-6 in the experimental processing conditions.

Moreover, a comparison between the P/N atomic ratios of the blend (arising from the chemical analysis of PA-6/EVA8/APP), of the raw materials mixture and of the material surface (Table 3) shows that APP and, as a consequence, PA-6 is not distributed in a homogeneous way in the blend. Moreover, the comparatively high surface P/N atomic ratio (the value of the ratio approaches 1, characteristic of the P/N of APP) proves either the migration of APP toward the surface of the material or the upholding of surface APP in a superficial EVA-8 rich phase.

The CP/DD-MAS NMR ^{13}C spectra of PA-6, EVA8 and PA-6/EVA8/APP are presented in Fig. 10. The PA-6 spectrum absorption bands have been previously assigned [48]. The EVA8 spectrum presents two bands assigned to ethylenic carbons with different conformations of the polymer chain (γ-left effect on carbon in the amorphous phase [49]). The chemical shifts of absorptions observed in PA-6/EVA8/APP are ascribable to PA-6 and EVA8 without any significant chemical modification of the virgin polymers. The proposed formation of aromatic (polyaromatic) species is not shown by the analysis because low amount of aromatic carbon or presence of linkage between the polyaromatic species.

The comparison of the MAS NMR ^{31}P spectra of APP ($\delta = -20$ ppm, characteristic of P–O–P bindings, Fig. 11) and PA-6/EVA8/APP (Fig. 12) shows that blending leads to the formation of orthophosphates ($\delta = 0$ ppm) and pyrophosphates species ($\delta = -10$ ppm) [13]. Breaking of the long polyphosphate chain into shorter chains can be explained by the thermo-mechanical stress sustained by the material in the

Table 3
Comparison of P/N atomic ratios of the initial raw materials mixture, of the PA-6/EVA8/APP blends and of its surface

Sample	P/N atomic ratio (in raw materials)	P/N atomic ratio (bulk analysis)	P/N atomic ratio (surface from XPS)
PA-6/EVA8/APP	0.48	0.38	0.79
APP	1.04	1	–

mixer, by an hydrolysis process via a reaction with water dissolved in the virgin PA-6 and/or the previously proposed reaction between the polyphosphate and PA-6 in the blending experimental conditions.

3.3. Structure characterization

The XRD study (Fig. 13) shows that the polymeric materials studied are both amorphous and crystalline and that APP is a crystalline compound. PA-6 spectrum presents two diffraction rays assigned to the (200) and (002;202) planes of the allotropic variety α of PA-6, respectively for $d = 0.441$ nm ($2\theta = 20°$) and $d = 0.375$ nm ($2\theta = 23.7°$) [50,51]. They are superimposed to a broad signal attributed to the X-ray scattering by the amorphous phase of the polymer.

The EVA8 spectrum is distinguished by a intense ray ($d = 0.415$ nm, i.e. $2\theta = 21.4°$) and a smaller one ($d = 0.378$ nm, i.e. $2\theta = 23.5°$). These rays are found again on the spectra of the blends (the smallest signal of EVA8 will nevertheless be ignored in the following study as it cannot be accurately discriminated from the experimental background).

Every diffraction rays of APP are observed in the blend; One additional diffraction ($2\theta = 15.16°$) may be assigned to mono-ammonium orthophosphate $NH_4H_2PO_4$ [50] (the previously characterized pyrophosphate species are not crystalline and are not observed using XRD). It has been previously observed that this species forms both with organic phosphates with short P–O–P chains during compounding of intumescent polymeric formulations via the reaction of APP with a carbonizing agent (polyol, starch [52]). Moreover, the breaking of the APP chain under the combined action of heat and shear stress may be assumed with a subsequent reaction with water dissolved in PA-6 (1–6 wt% relative to PA-6 depending on the laboratory conditions).

Moreover, Table 4 shows that the inter-reticular distances d_{200} and $d_{002-202}$ of PA-6 and d_{EVA} does not change versus the APP content. So, it may be assumed that low molecular weight phosphate or phosphocarbonaceous species are not

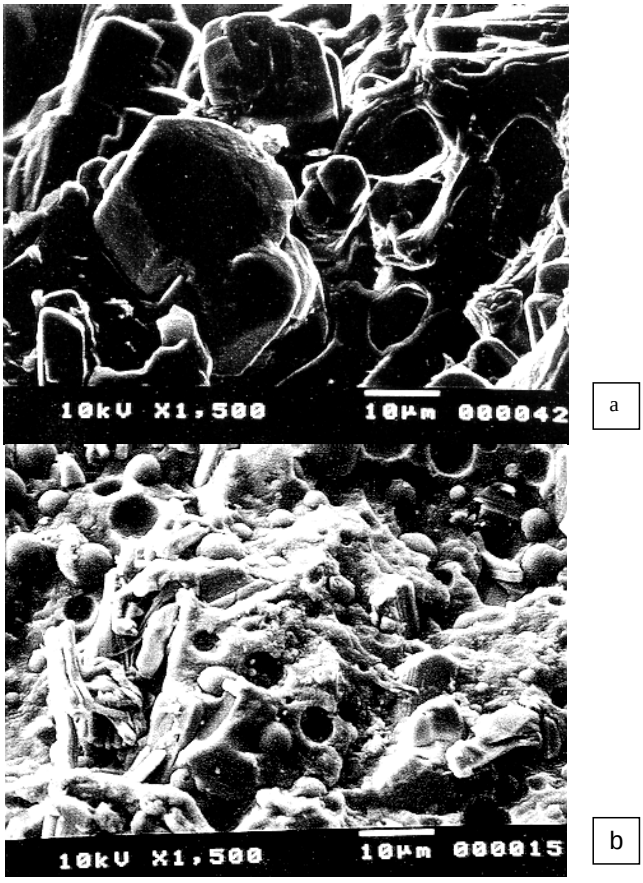

Fig. 9. SEM picture of fractures of (a) PA-6/APP 28% and (b) PA-6/EVA8/APP.

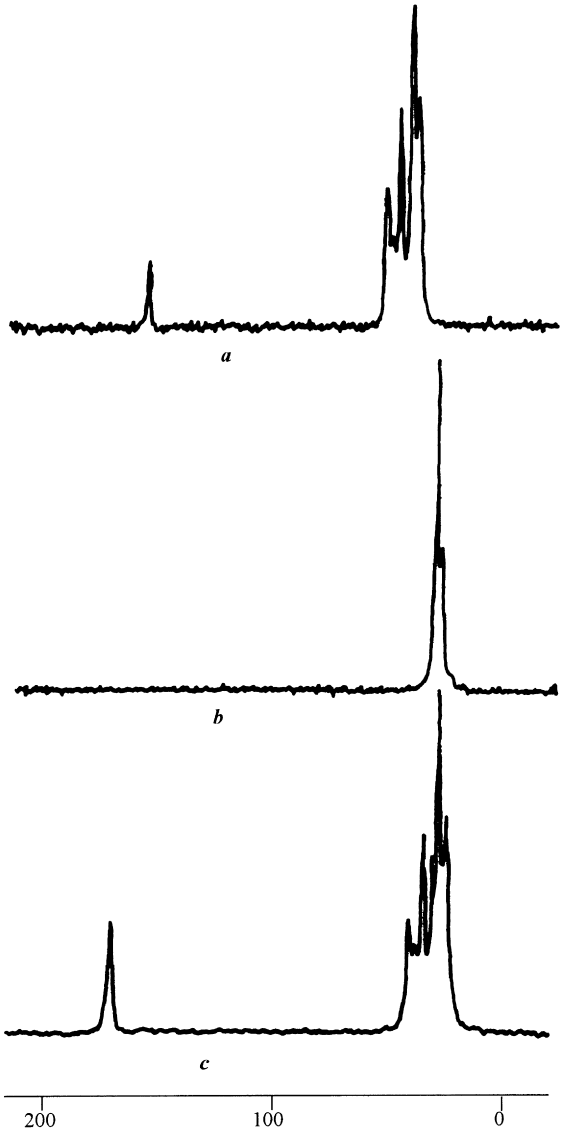

Fig. 10. ^{13}C CP-DD-MAS RMN spectra of (a) PA-6; (b) EVA8; and (c) PA-6/EVA8/APP.

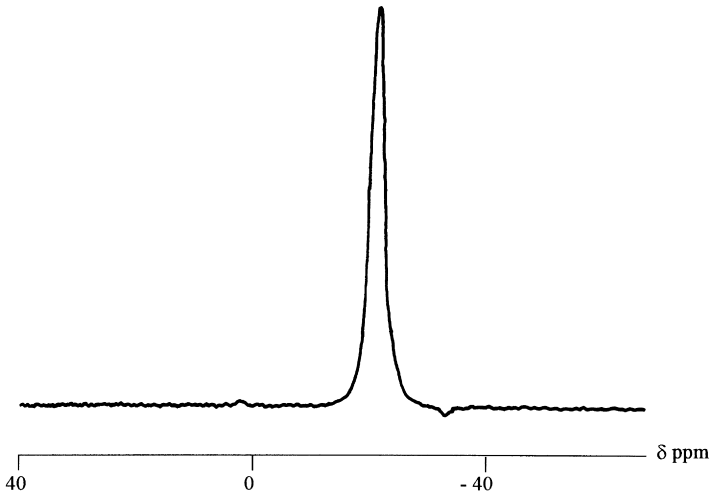

Fig. 11. ^{31}P MAS RMN spectrum of APP.

inserted in the polymers crystalline phases. The mean size of the PA-6 crystal in the blend is slightly lower than this one of the virgin PA-6 (Table 4). Fig. 14 shows that this effect is only observed with 25–28 wt% addition of APP.

The ratio between the polymers crystalline phases and amorphous phases (c/a; computed using the protocol of Murthy et al. [51] after subtraction of the diffraction rays of the phosphate phases) very close to this one of the virgin PA-6, seems to imply that the semi-crystalline state of the polymer is preserved in PA-6/EVA8/APP. It may be noticed that blending PA-6 and EVA8 in our experimental conditions leads to a comparative decrease of the amorphous character of this material (Fig. 15) and that addition of APP in this blend decreases the amount of the polymeric crystalline phases in the blend.

The change of the PA-6 and EVA8 intrinsic crystallinities can be studied considering the respective intensities of the rays (only the main diffraction ray of EVA8 ($2\theta = 21.4°$) and the two rays characteristic of PA-6 ($2\theta = 2°$ and $23.7°$) are considered). The useful penetration depth of the X-rays in the material, taken into account here, allows the calculation of the diffracting volume and then the corresponding polymer amount (signal are given in photo-multiplied counts per *g*, labeled u.a. in the text).

Blending the PA-6/EVA8 6/1 mixture leads to an apparent conservation of the crystallinity of the PA-6 phase with a weak isotropy proved by the decrease of the $I_{200}/I_{002,202}$ ratio, and a decrease of the crystallinity of the EVA8 phase (Table 5).

In the PA-6/EVA8/APP blends, EVA8 crystallinity initially increased by addition of low amounts of APP, then decreases for APP contents higher than 15 wt%. Moreover,

Table 4
Structural data of PA-6, EVA8 and PA-6/EVA8/APP

Samples	d_{200} (PA-6) (nm)	$d_{002-202}$ (PA-6) (nm)	d (EVA8) (nm)	c/a ratio	Particle size (nm)
PA-6	0.443	0.374		0.67	9.40
EVA8	–	–	0.417		
PA-6/EVA8/APP	0.441	0.374	0.414	0.66	8.91

Table 5
Intrinsic intensities of the characteristic polymer diffraction rays in the materials

Formulation	I_{200} (PA-6) (u.a.)	$I_{002-202}$ (PA-6) (u.a.)	I (EVA8) (u.a.)
PA-6	0.0232	0.0592	–
EVA8	–	–	0.0719
PA-6/EVA8 6/1	0.0250	0.0436	0.0592
PA-6/EVA8/APP 15%	0.0387	0.0720	0.0781
PA-6/EVA8/APP 20%	0.0282	0.0573	0.0632
PA-6/EVA8/APP 25%	0.0375	0.0756	0.0537
PA-6/EVA8/APP 28%	0.0348	0.0800	0.0586
PA-6/EVA8/APP 50%	0.0428	0.0892	0.06

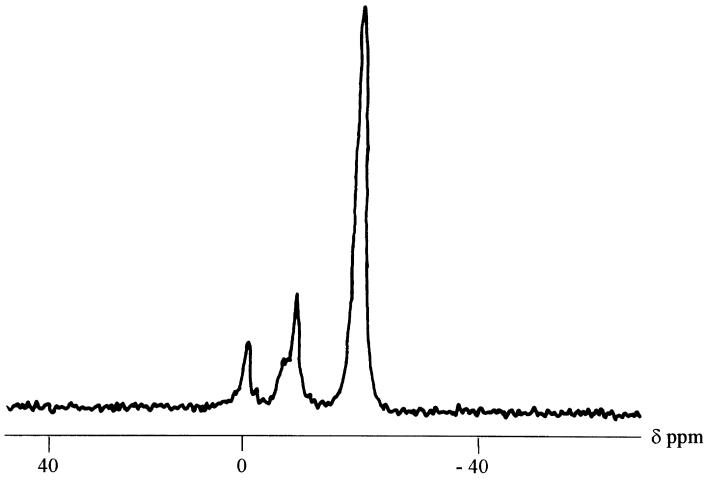

Fig. 12. ^{31}P MAS RMN spectrum of PA-6/EVA8APP.

addition of APP always leads to a significant increase of the crystallinity of the PA-6 phase and lowers the I_{200}(PA-6)/$I_{002,202}$(PA-6) ratio (Fig. 16), this low value giving evidence of a preferential orientation of the PA-6 crystals in PA-6/EVA8/APP.

The significant increase of the intrinsic crystallinity of the PA-6 phase and the decrease of the crystalline phase/amorphous phase ratio in PA-6/EVA8/APP seems to be contradictory results. This may not be only explained by the relatively low loss of crystallinity of the EVA8 phase. So, it implies that, as previously proposed, APP and PA-6 partially degrades during compounding and that the corresponding products (hydrolyzed phosphate species with short P–O–P chains, organic phosphates and aromatic species) are components of the amorphous phase of the blend.

3.4. Microscopic structure and molecular dynamic study

^{1}H NMR study using the method of inversion recovery [π–τ–π/2], shows that only one spin–lattice relaxation time T_1 value is observed for each formulation (Table 6). This result implies that the polymeric systems do not present any structural heterogeneity with a size higher than 10 nm [53–56].

Spin–spin relaxation times in the materials are then considered. The free precessions of the systems have been recorded using a spin-echo sequence [57]. In each case, they present complex shapes. In a first assumption, two decays may be distinguished: one fast and the second slower (Table 7). The fast decaying component is assumed to be Lorentzian and the slow decaying component is described by functions 1 (combination of a Gaussian and a Weibullian), 2 (Gaussian) or 3 (combination of a Gaussian and a Lorentzian) [58]:

Table 6
Spin–lattice relaxation times of the polymeric materials

Sample	T_1 (ms)
PA-6	495
EVA8	278
PA-6/EVA8	348
APP	1970
PA-6/EVA8/APP	520

1. $M = M_{0C}\exp(-(t/T_{2C})^e) + M_{0L}\exp(-(t/T_{2L})^2)$

2. $M = M_0\exp(-(t/T_2)^2)$

3. $M = M_{0C}\exp(-(t/T_{2C})^2) + M_{0L}\exp(-t/T_{2L})$

where t is the time, M_{0C} and M_{0L} are, respectively, the magnetization amplitudes of the fast and slow decaying components, T_{2C} and T_{2L} are, respectively, the spin–spin relaxation times of the fast and slow decaying components and e the Weibull coefficient ($1 < e < 2$) [59]. The function $\exp(-(t/T_{2C})^2$ allows the adjustment of FID which components are intermediates between Gaussian and Lorentzian ones [58].

APP presents only one decay, which is easily explained by its rigid crystalline structure which implies a fast decay. Moreover, two T_2 values are observed from each polymeric sample and the presence of two phases in these materials is thus demonstrated. A previous XRD study has shown that virgin polymer and the polymers in blends present a semi-crystalline structure. In such a structure, the fast component may be assigned to the crystalline phase and the slow decaying component to fast molecular motion of the protons in the amorphous phase. The comparatively low value of the PA-6/EVA8/APP T_{2L} shows that the rigid character of the amorphous phase is decreased by addition of APP in the PA-6/EVA8 blend.

M_{0C} and M_{0L} values are directly related to the relative proton contents in respectively, the crystalline and the amorphous phase. It is to be noticed that processed EVA8 possesses 90% of its protons in an amorphous/mobile phase. This result is inconsistent with the about 70% crystallinity of the virgin material as measured using XRD. It may be assumed that the degradation of this polymer occurs in

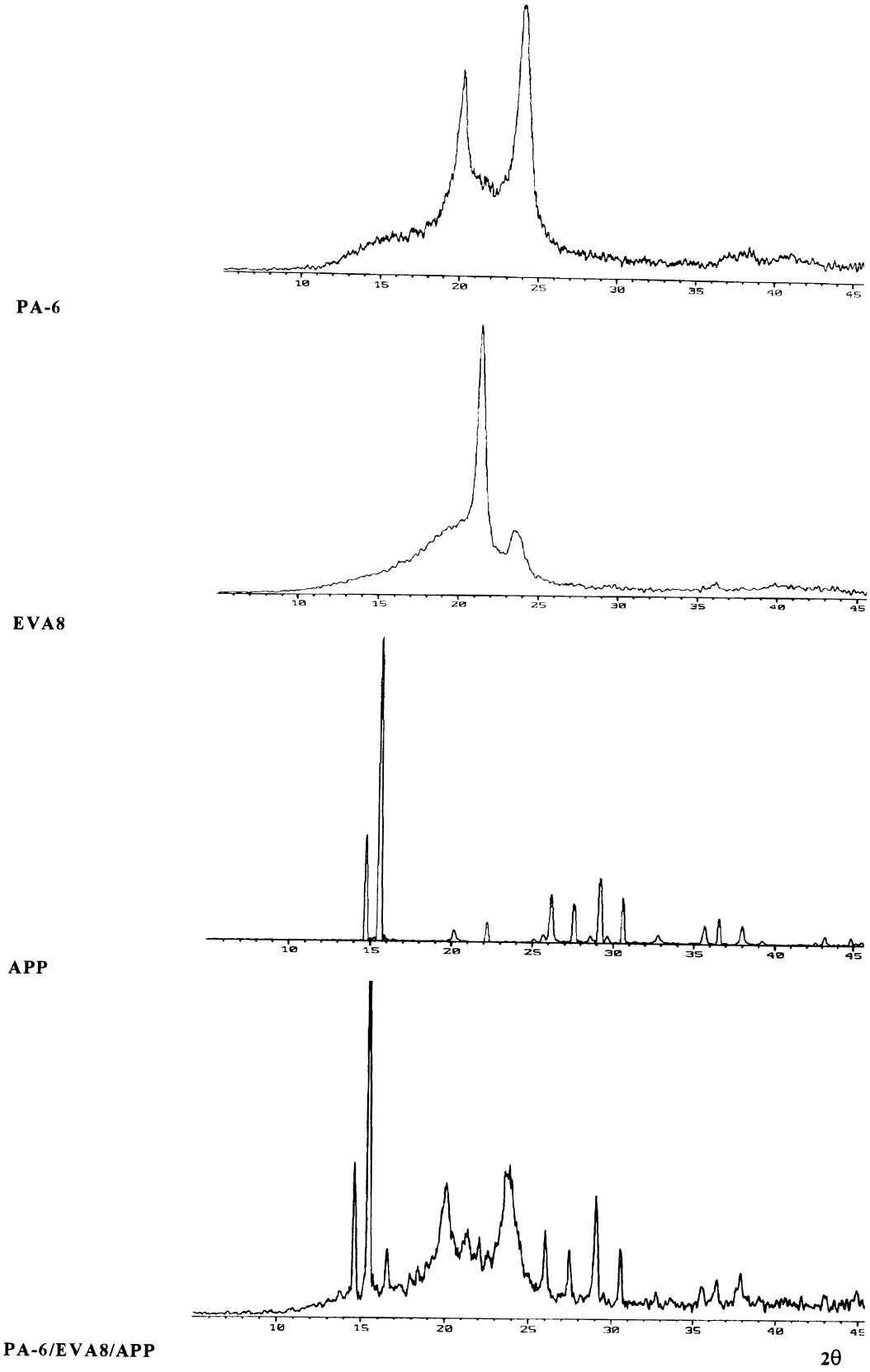

Fig. 13. XRD spectra of the raw materials and PA-6/EVA8/APP.

Table 7
Simulations of the FID of the virgin APP, the processed polymers and the polymeric blends

Sample	Function	M_{0C} (%)	M_{0L} (%)	T_{2C} (μs)	T_{2L} (μs)	e
PA-6	1	86.4	11.0	9.2	55.3	1.6
APP	2	99.0		31.8		
EVA8	3	10.2	89.8	10.2	27.7	
PA-6/APP	1	69	31	10.4	29.8	1.7
PA-6/EVA8	1	74.9	25.1	10.04	51.7	1.5
PA-6/EVA8/APP	1	70.9	28.1	10.7	37.4	1.5

the processing conditions (235°C during 1200 s). The resin resulting from this degradation process, stays as an amorphous phase in the final material; decrease of the length of the polymer chains preventing the increase of rigidity resulting from crosslinking between these chains.

Finally, the comparatively low relative amounts of protons in the crystalline phase of PA-6/EVA8/APP agrees well with its XRD study which shows a comparative decrease of its crystallinity. More, APP protons of residual APP and low chain phosphate species has to be considered as protons of the amorphous phase because it is commonly assumed that additives sit in the amorphous phase of a semicrystalline polymeric material [60].

Measurement of T_2 values gives information on the compatibility of materials: T_2 of a mixture equals to T_2 of a particular virgin component shows incompatibility of the mixture components [61]. Compatible compounds give mixtures with T_2 values between those of the virgin components.

The study considers only the T_{2L} values because APP does not present a fast decaying component. It confirms that APP and PA-6 are not compatible ($T_{2L\ \text{PA-6/APP}} \approx T_{2\ \text{APP}} < T_{2L\ \text{PA-6}}$]) and that addition of both EVA8 and APP in PA-6 gives a compatibilized mineral–polymer compound ($T_{2L\ \text{PA-6/EVA8/APP}} \in [T_{2L\ \text{EVA8}}, T_{2L\ \text{PA-6}}]$ and ($T_{2L\ \text{PA-6/EVA8/APP}} \in [T_{2\ \text{APP}}, T_{2L\ \text{PA-6}}]$).

The $\bar{b}$ (mean width of the domain undergoing slow relaxation) values were finally computed from spectra using Goldman–Shen sequences [35] using the theory developed by Cheung and Gerstein [40]. They are deduced from adjustments of the recovery factor $R(t)$ during curve fits, as discussed in Ref. [15].

Table 8 shows that addition of EVA8/APP in PA-6 increases the size of the amorphous domain. In the PA-6/EVA8/APP study, adjustment of $R(t)$ with $\bar{b}$ considering a $\bar{b}$ Gaussian distribution is not possible. Fit of the experimental curve is only possible using Poisson's law. It may be recalled that Gaussian distribution corresponds to a "packets" repartition of the signal with different $\bar{b}$ values and that Poisson distribution correspond to an homogeneous distribution of the signal and then of the size of the domains. So, an homogeneous repartition of the amorphous phase in the blend may be assumed.

To conclude, NMR study has shown that addition of APP in the polymeric matrix does not lead to a chemical change of the polymer chains. The phosphate species location in the amorphous domains of the matrix may explain the increase of the size of the amorphous domains. More, the study shows that EVA8 in the blend allows the compatibility of APP in the polymeric matrix. It may be proposed that the amorphous character of EVA8 (93% of the protons belonging to its amorphous domain in the processing conditions) allows the easy location of APP in the blend.

From literature [62], formation of a blend of two semicrystalline polymers leads to the presence of two different phases, i.e. the presence of both a mixture of the two amorphous phases and of a homogeneous mixture of the crystalline and a amorphous phase. The existence of these two phases in the blend is verified considering the T_2 values.

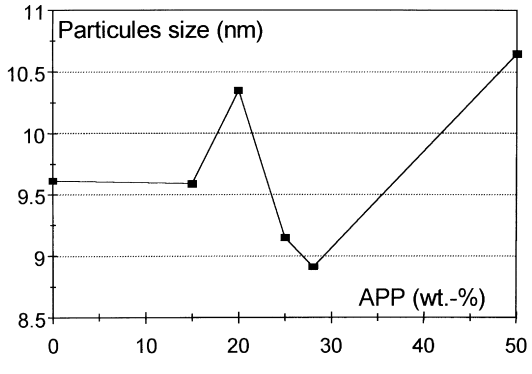

Fig. 14. PA-6 crystal mean size in blends (PA-6/EVA8 = 6, w/w) versus their APP content.

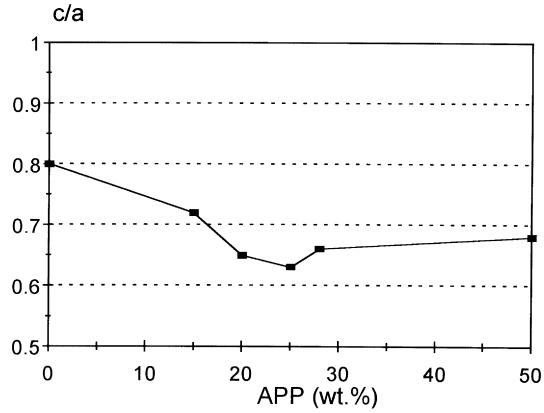

Fig. 15. c/a ratio in blends (PA-6/EVA8 = 6, w/w) versus the APP content.

Table 8
Spin-diffusion coefficient, average of the distance between two protons (a deduced from XRD spectra) and $\bar{b}$ size of the slow relaxation domains

Formulations	D (cm^2/s)	a (nm)	$\bar{b}_{3D}$ (nm)
PA6	1.31×10^{-8}	0.959	1.9
PA6/EVA8/APP	1.10×10^{-8}	0.955	2.8

Moreover compatibility of an additive in a polymeric matrix may be achieved using a functionalized copolymer which acts as a covering agent [62]: EVA8 first plays the part of a "capsulation" agent of APP particles which locate then in the amorphous phase of PA-6. APP particles covered by EVA present a comparatively large size which may explain the observed increase of the amorphous domains mean size.

4. Conclusion

The study specifies the blending conditions for an FR intumescent additive master batch in which polyamide-6 is the carbonization agent and ammonium polyphosphate is the carbonization catalyst. The problem of the migration of the phosphate throughout the polymeric matrix is discussed. It is shown that addition of relatively low amount of a functionalized polymer (an ethylene–vinyl acetate copolymer is used in the study) may avoid this migration. ^{1}H NMR spectroscopy is presented as a tool to predict and to explain the part played by this compatibilizer.

Acknowledgements

The authors gratefully acknowledge the Conseil Régional du Nord-Pas de Calais, the Conseil Général du Pas de Calais, C.E.A.C. (Péronne, France) and Taraflex (Tarare, France) for their financial support. They are indebted to F. Poutch (CREPIM, Bruay-la-Bussière, France) and B. Revel (Centre Commun. RMN, U.S.T.L., Villeneuve d'Ascq, France) for their skilful assistance in, respectively, processing and solid state NMR experiments and to Dr. L. Gengembre (UPRES A CNRS 8010, U.S.T.L., Villeneuve d'Ascq, France) for helpful discussion of XPS data.

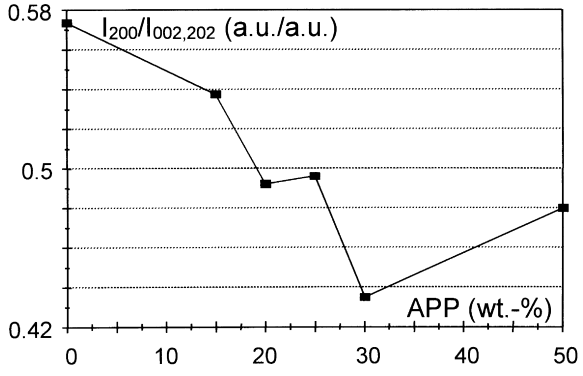

Fig. 16. PA-6 $I_{200}/I_{002,202}$ ratio of PA-6/EVA8/APP versus APP content.

References

[1] Vogel H. In: Hüthig A, editor. Flammfestmachen von Kunsthoffen, Heidelberg: Springer, 1966.
[2] Lyons JW. The chemistry and uses of fire retardants, New York: Wiley Interscience, 1970.
[3] Bhatnagar VM. Flame retardant formulation handbook, Westport: Technomic, 1972.
[4] Howarth JT, Lindstrom RS, Sheth SG, Sidman KR. Plast World 1973;March:65–73.
[5] Bieniek D, Bahadir M, Korte F. Heterocycles 1989;28(2):719–22.
[6] Pinkerton MN, Kociba RJ, Petrella RV, McAllister DL, Willis ML, Fulfs JC, Thoma H, Hutzinger O. Chemosphere 1989;18(1–6):1243–9.
[7] Dumler R, Lenoir D, Thoma H, Hutzinger O. Chemosphere 1990;20(10–12):1867–73.
[8] Clausen E, Lahaniatis ES, Bahadir M, Bieniek D. Fresenius J Anal Chem 1987;327:297–300.
[9] Fifth Draft Status Report OCDE Workshop on the Risk Reduction of Brominated Flame Retardants, Neufchâtel, Switzerland, 26th May 1992, 22–25 February 1993, OECD-Environment Direction, April 1993.
[10] Preliminary 1st Draft Report International Programme on Chemical Safety—Environmental Health Criteria for Brominated Diphenylethers (January 1993), 1st Draft Report International Programme on Chemical Safety—Environmental Health Criteria for Tris(2,3-dibromopropyl) phosphate and Bis(2,3-dibromopropyl) phosphate (January 1993), United Nations Environmental Programme, PCS/EHC/92.45, non-edited reports.
[11] Kroenke WJ. J Mater Sci 1986;21:1123–73.
[12] Camino G, Costa L, Trossarelli L. Polym Degrad Stab 1984;7:25.
[13] Delobel R, Le Bras M, Ouassou N, Alistiqsa F. J Fire Sci 1990;8(2):85.
[14] Le Bras M, Bourbigot S, Delporte C, Siat C, Le Tallec Y. Fire Mater 1996;20:191.
[15] Bourbigot S, Le Bras M, Delobel R, Descressain R, Amoureux J-P. J Chem Soc Faraday Trans 1996;92(1):149.
[16] Bourbigot S, Delobel R, Nathiez P, Bréant P. Compositions ignifugeantes pur mélanges de résines thermoplastiques contenant une zéolithe et mélanges de résines thermoplastiques renfermant lesdites compositions, EU patent no. 94.401317.8 by ELF Atochem S.A., 1994; P. Nathiez, Amélioration du comportement au feu de l'orgalloy R6000 par un système intumescent, Mémoire au Conservatoire National des Arts et Métiers (available GéPRIM, ENSCL), Villeneuve d'Ascq, 1991.
[17] Levchik SV, Costa L, Camino G. Polym Degrad Stab 1992;36:229–37.
[18] Bourbigot S, Le Bras M, Siat C. Use of polymer blends in flame retardancy of thermoplastic polymers. In: Lewin M, editor. Recent advances in flame retardancy of polymeric materials, 8. Norwalk: Business Communications, 1998. p. 146–60.
[19] Siat C, Bourbigot S, Le Bras M. Structural study of the polymer phases in intumescent PA-6/EVA/FR additive blends. In: Lewin M, editor. Recent advances in flame retardancy of polymeric materials, 7. Norwalk: Business Communications, 1997. p. 318–26.
[20] Le Bras M, Bourbigot S. Unpublished results.
[21] Standard test method for measuring the minimum oxygen concentration to support candle-like combustion of plastics, ASTM D2863/77, Philadelphia.
[22] Tests for flammability of plastic materials for parts in devices and appliances, Underwriters Laboratories, Northbrook, ANSI/ASTM D635-77.
[23] Le Bras M, Bourbigot S. In: Karger-Kocsis J, editor. Intumescent fire

retardant polypropylene formulations in polypropylene: an A–Z reference, London: Chapman and Hall, 1998.
[24] Babraukas V. Development of the cone calorimeter–a bench scale rate of heat release based on oxygen consumption, NBS-IR 82-2611, US National Bureau of Standards, Gaithersburg, 1982.
[25] Bourbigot S, Le Bras M, Bugajny M, Dabrowski F. Intumescence and polymer blending—an approach for flame retardancy. In: Beall KA, editor. Book of Abstracts. NIST Annual Conference On Fire Research, 2–5 November, 1998, NISTIR 6242, Gaithersburg: US Department of Commerce, 1998. p. 43–44.
[26] Siat C, Le Bras M, Bourbigot S. Fire Mater 1998;22:119–28.
[27] Le Bras M, Bourbigot S, Siat C, Delobel R. Comprehensive study of the protection of polymers by intumescence—application to ethylene vinyl acetate copolymer formulations. In: Le Bras M, editor. Fire retardancy of polymers—the use of intumescence, Cambridge, UK: Royal Society of Chemistry, 1998. p. 266–80.
[28] Felix E. Etude structurale par RMN du solide de formulations ignifugeantes à base de PA-6, Diplôme d'Etudes Approfondies Dissertation (available GéPRIM), Lille, 1995.
[29] Pouille F. Etude Spectroscopique de Formulations "Retard au Feu" à base de Polyamide, Diplôme d'Etudes Approfondies Dissertation, (available GéPRIM), Lille, 1995.
[30] Blyler LL, Daane JH. Polym Eng Sci 1967;7:178–81.
[31] Lee GC, Purdon JR. Polym Eng Sci 1969;9(5):360–4.
[32] van Wazer JR, Lyons JW, Kim KY, Colwell RE. Viscosity and flow measurement—a handbook of rheology, New York: Wiley, 1963.
[33] Poutch F. Mesure de la Viscosité de Formulations Rhéologiquement Complexes, Mémoire du Conservatoire National des Arts et Métiers (available GéPRIM), Dissertation, Lille, 08 April 1998.
[34] Poutch F, Le Bras M, Bourbigot S, Delobel R. In: Loucheux C, editor. Résumé du 28ème Colloque National Annuel du GFP—Polymères et Futur, Lille, France, 17–19 november 1998, Lille: GFP Pub, 1998 paper C07.
[35] Beamson G, Briggs D. High resolution XPS of organic polymers, Chichester: Wiley, 1992.
[36] Lemaitre JL, Goving Menon P, Delannay F. In: Delannay F, editor. Heterogeneous catalyst, 15. New York: Marcel Dekker, 1984. p. 299.
[37] Raymond SA. Electron paramagnetic resonance, New York: Wiley Interscience, 1968 p. 200.
[38] Powels JG, Strange JH. Proc Phys Soc 1963;82:6.
[39] Golman M, Shen L. Phys Rev 1966;144:321.
[40] Cheung TTP, Gerstein BC. J Appl Phys 1981;52:5517.
[41] Bloembergen N. Physica 1949;15:386.
[42] Levchik SV, Costa L, Camino G. Polym Degrad Stab 1992;36:229.
[43] Levchik SV, Camino G, Costa L, Levchik GF. Fire Mater 1995;19:1.
[44] McNeill IC, Jamieson A, Tosh DJ, McClune JJ. Eur Polym J 1976;12:305.
[45] Lewis IC, Singer LS. Carbon 1967;5:373.
[46] Lewis IC, Singer LS. J Phys Chem 1981;85:354.
[47] Fontanille M, Gnanou Y. In: Chatain M, editor. Structure Moléculaire et Morphologie des Polymères, Traité Matériaux non métalliques, Techniques de l'lngénieur, Paris, 1995, p. 25–7.
[48] Weeding TL, Veeman WS, Gaur HA, Huysmans WGB. Macromolecules 1988;189(7):2028.
[49] Hartfield GR, Glans JH. Polym Prepr ACS Div Polym Chem 1990;31(1):151.
[50] Murthy NS. Polym Commun 1991;32(10):301–5.
[51] Murthy NS, Minon H. Polymer 1992;31(6):996.
[52] J.C.P.D.S., file number 27-0062.
[53] Bloembergen N. Physica 1949;15:386.
[54] Abragam A, Goldman M. In: Abragam A, editor. Nuclear magnetism: order and disorder, New York: Oxford University Press, 1982.
[55] McBrierty J, Douglass DC. Phys Rep 1980;63:63.
[56] McBrierty J, Douglass DC. J Polym Sci Macromol Rev 1981;16:295.
[57] Tanaka H, Nishi T. J Chem Phys 1985;82(9):4326.
[58] Kaufman S, Bunger DJ. J Magn Reson 1970;3:218.
[59] Weibull W. J Appl Mech 1951;73:293.
[60] Schlotter NE, Furlan PY. Polymer 1992;33(16):3323.
[61] Kosfeld RH, Zumkley L. MMI Press Symp Ser Polym Compat Incompat 1992;2:2213.
[62] Steward ME. Fundamentals of polymer blend technology—fire retardant blends, alloys and thermoplastic elastomers. Spring Conference, Society of Plastics Engineers, PMAD Division and FR Chem. Association, 1991.